INTEGRATION OF EEG AND MRI DATA OF INDIVIDUAL BRAIN

DOROTA KOZIŃSKA[1], KRZYSZTOF NOWIŃSKI[2],
ANNA KOŁODZIEJAK[1], REMIGIUSZ TARNECKI[1]

[1]*Nencki Institute of Experimental Biology, Warsaw, Poland*
[2]*Interdisciplinary Center for Mathematical and Computational Modeling, Warsaw, Poland*

Abstract: Accurate spatial localization of areas of pathological activity in the brain cortex is of great importance for studying processes of generation and propagation of electrical signals in the brain both in research and in clinic. This paper presents a method providing superposition of data acquired in EEG or EP examination with a patient's cortical surface computed from MR images. To integrate electrophysiological information with MRI-scanned anatomy scalp electrodes are registered with the cortex surface using distance based alignment technique. This approach is automatic and does not require any external fiducial markers to be fixed on a patient's head. It uses geometrical features derived from intrinsic image data to guide the alignment. That is why the method is easy to apply to numerous examinations in clinic. Once data are registered, they are fused and rendered in 3D space as colour surface maps. The usefulness of the method for neurological assessment is demonstrated by presenting results of EEG and SEP studies performed on two patients.

1. Introduction

The recent developments in brain mapping are constantly creating opportunities for better understanding topographic aspects of the motor and sensory functions of the cerebral cortex both in research and in clinic. Electroencephalography complemented with other modalities like, MRI, PET, SPECT is tending to localize both normal and pathological electrical activity more precisely. For many years EEG techniques (including evoked potentials) have been used as the initial diagnosis for many neurological diseases.

Initially, curves representing electrical signals recorded from human scalp were difficult to interpret in spatial relation studies. Brain Electrical Activity Mapping (BEAM) techniques introduced by Duffy 1986 (9) provided definitely a better tool for analyzing brain functions and have been widely used for visual inspection. These techniques transform apparently complex waveforms into surface distributions, which are presented on some standard disc/ellipse representing the brain surface. Moreover, they assume some standard locations of electrodes, constant for all brains. Since accurate localization of pathological foci in the relation to

anatomical structures is of great importance for surgery and treatment planning, it is reasonable to combine electrophysiological data with the information revealing the brain anatomy.

So far MR images of the brain provide the best reference to estimate spatial localization and extent of pathology in the individual living humans. Following this idea we have developed a system facilitating superposition EEG/EP on MRI information and presentation of electrical activity distribution on the cortical surface of the examined subject. The cortical surface is computed from MRI data. Our method provides simultaneous observation of functional (electrical activity) and anatomical information about the currently studied brain. Thus, it avoids an error resulting from variability of individual topography of the cortex. Moreover, it allows the user to be flexible about choosing electrode positions on the scalp.

Simultaneous visualization of functional and anatomical data requires two steps; registration (alignment of data by means of geometric transformation) and fusion (visualization of the joint results). This work focuses on developing the technique for registration of EEG/EP and MRI data sets. The method is automatic and doesn't require any external fiducial markers to be placed on a patient's head, since it uses geometric features derived from the intrinsic image data to guide the alignment. It makes the studies easy especially when numerous EEG/EP and MRI examinations are performed at different places and times or we need to compare EEG/EP performed at different times. The method follows the idea of distance based alignment.

This work does not approach the problem regarding distortion of electrical signal during propagation from cortex to scalp surface. During the propagation from the cortex towards the scalp surface potentials are attenuated, distorted and spread due to different conductivities of the neural tissue, cerebro-spinal fluid, meninges, skull and scalp (Nunez 1986 (31), Nunez 1995 (32)). As a result, the distribution of EEG potentials over the scalp has a low spatial resolution. This resolution can be increased with methods that significantly reduce the spatial blur of the potential. Since the objective of this work is to deal with standard examinations performed in clinic, the common 10-20 system (20 electrodes) available in our Lab is used. According to recent works proposing solutions of this problem (Dale 1993 (6), Gencer 1996 (9), Yvert 1996 (26), Babiloni 1997 (1)) it seems that the usage of electrodes of number equal 20 is too small for such studies. That is why no high resolution studies are pursued here, and no deblurring technique is applied. The spherical spline method is used to interpolate potential distribution on the cortical surface.

To demonstrate the usefulness of the method we present the results of studies of two our patients: one for EEG, and one for evoked potentials.

2. Method

From MRI examination we obtain a set of crossectional images of the patient's head in arbitrary cutting plane. Scalp and cortex boundaries are detected from them. A stack of contours is used to compute 3D coordinates of scalp and cortex surface points. A patient is also subjected to EEG/EP examination, from which we gather

values of electrical potentials recorded with scalp electrodes, as well as 3D coordinates of electrodes. To localize electrodes in the relation to the cortex surface we have to bring these two objects into a common coordinate system, i.e. to align them. This involves determination of a geometric transformation, which will transform one or both data sets. Subsequently, interelectrode potentials are interpolated for all points of the cortex surface and corresponding colours are assigned to them. The coloured surface is rendered and manipulated in 3D space as needed.

Software for data preprocessing, 3D alignment and potential interpolation was written in C and added to AVS (Advanced Visual Systems Inc.) package as modules running on SGI/Sun machine. 3D rendering of electrical activity distribution is performed using modules provided by AVS.

Data Acquisition

A set of 64 crossectional images of the head was scanned every 3 mm for each patient. Siemens Magnetom 1.5T scanner was used in Turbo SE sequence and T1 weighted images were scanned. The scale of each image was 1mm/pixel. Sets of 64×256×256 images were transmitted from VAX to SGI machine.

In electrophysiological examination patients were put into an electromagnetically shielded cage, lying in a relaxed position with closed eyes. 20 electrodes were placed on their scalps according to 10-20 system. 3D coordinates of electrodes were measured during the examination for each patient individually. Electrical potential values were recorded with 20 channels, amplified (Grass Model 12 Neurodata Acquisition System), digitized (12-bit AD converter) and transmitted to IBM PC. The electric reference was set on linked ear lobes for EEG and on a forehead for SEP. In sensory evoked potential examination a patient's median nerves were stimulated with a square-wave constant current pulses of amplitude about 5-7 mA, duration of 0.3 ms and rate of 1.5 Hz. Stimulations were given to the median nerves at the wrists. The intensity of the stimulus was adjusted to determine a painless muscle twitch of the thumb. 256 sweeps were averaged for each stimulation. Sampling frequency was 2 kHz for SEP and 128 Hz for EEG signals. Collected data were transmitted to SGI machine.

Preprocessing

The X-Y (in-plane) resolution of original MR images was 1 mm/pix, while scan increment (in Z axis) was 3 mm. To obtain a regular hexahedral grid missing planes between original images were interpolated linearly. In the next step scalp boundaries were extracted from original images using a single threshold (Fig. 1a). Cortex boundaries were extracted using interactive region growing algorithm (Fig. 1b). Subsequently, 3D coordinates of their surface points were computed (Fig. 1c, 1d).

3D Alignment

To localize electrodes in the relation to MRI cortex surface laying in a different coordinate system we have to align (register) these two objects. This involves computation of geometric transformations, which will transform one or both objects into a common coordinate system. Numerous solutions approach this problem as

given by van der Elsen et al. 1993 (22). The algorithm we used to find the required transformation based on methodology for designing algorithms for multidimensional image alignments presented in (13). This approach is closely related to the method introduced by Levin et al. 1988 (16), as well as to the algorithm developed independently by Besl and McKay 1992 (3). They align two 3D data sets by minimizing the distance between them. Pelizzari et al 1989 (18) used this technique to align MRI, CT and PET data sets. Borgefors 1988 (4) presented the chamfer matching algorithm, which was used by Jiang et al. 1992 (12) to register 3D surfaces.

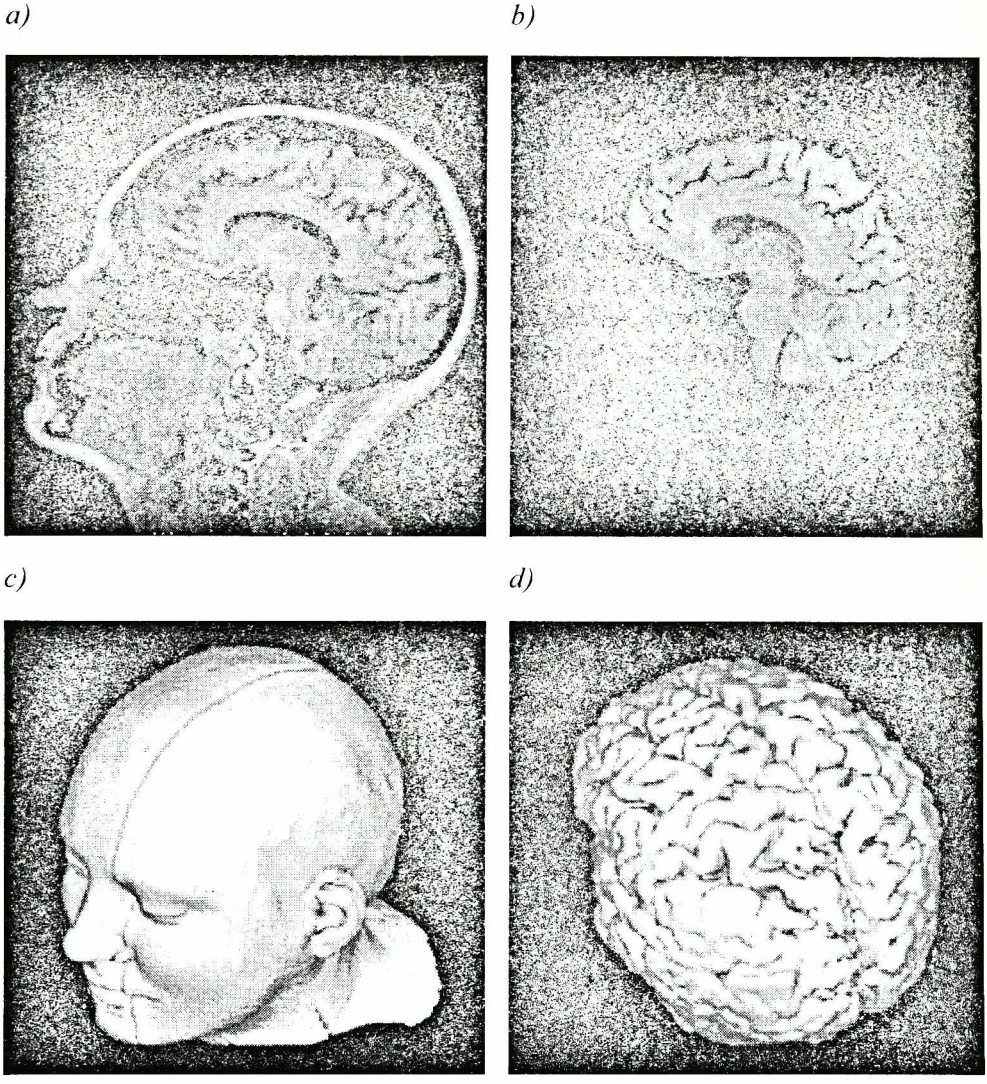

Figure 1. *MRI data preprocessing. a) Saggital crossection of the head, scalp contour segmented. b) Cortex contour segmented. c) A scalp surface computed from a stack of boundaries. d) Cortex surface computed from the stack of boundaries.*

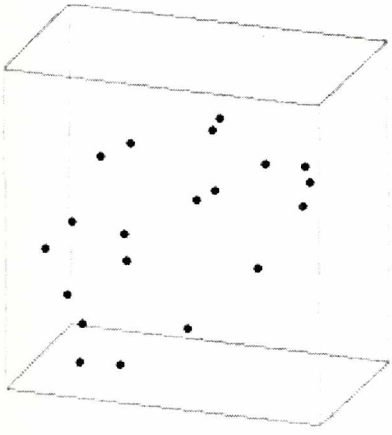

a)

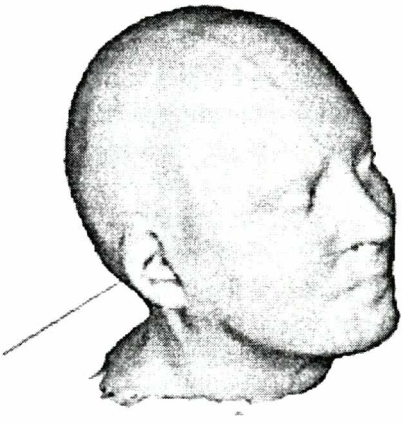

b)

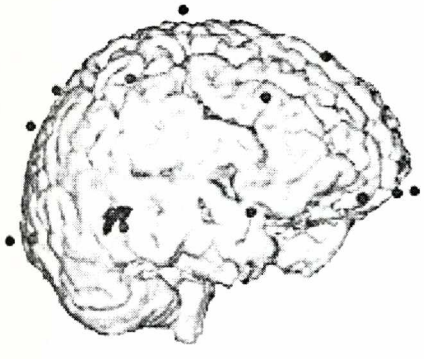

c)

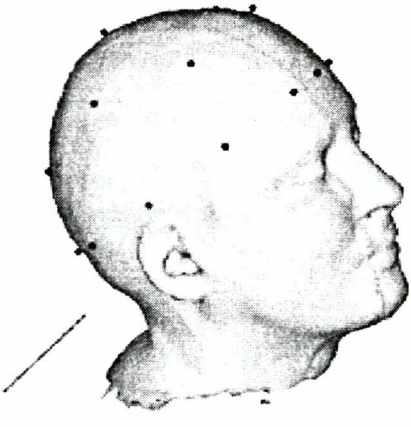

d)

Figure 2. *3D geometrical alignment. a) A test object: points. b) A reference object: scalp surface. c) Electrodes aligned to the scalp surface. d) Electrodes aligned to the cortex surface. Electrodes do not touch the cortex because they were placed on the scalp.*

The approach we have chosen is close to the ones mentioned above. It uses the intrinsic image data (here the head surface) to guide the alignment. Thus, it avoids the problem of fixing external fiducial markers or detecting anatomical landmarks except for organ surfaces. It makes the method easy to apply, especially when we deal with numerous examinations in clinic. The method assumes a rigid body transformation of objects to be aligned. Since we deal with a rigid body transformation

we can use a subset of data for the computation of the transformation and get sufficiently good alignment. Here we use 20 control points (electrode positions on the scalp).

Since scalp and cortex surfaces are in the same coordinate system, first we align electrodes to the scalp surface (Fig. 2c). Subsequently, the computed transformation is used to align electrodes to the cortical surface (Fig 2d).

The problem to be solved here is the following: given are two objects in 3D space: S_r — a reference object (here the head surface, Fig. 2b) and S_t — a test object (here 20 points representing scalp electrodes, Fig. 2a) i.e. the one to be aligned. We are looking for geometric transformation that aligns the test object with the reference one (Fig. 2c). Since both S_r and S_t are obtained experimentally, the lack of precision in surface segmentation and measurement of electrode positions may make them not possible to be aligned exactly. The method we have chosen proposes to tackle this problem by using a disparity function to measure the alignment error. If p' is a test point p transformed into a new location with a rigid body transformation F, then the disparity function $d(p',S_r)$ is defined as a distance between transformed point p and the data set S_r i.e. distance between transformed point p and the point closest to it, belonging to the object S_r. We define the alignment error for a set of points $S_t=\{p_1,...p_N\}$ with respect to a reference object S_r as:

$$e(S_t,S_r) = \sum_{i=1}^{N} d^2(p_i S_r) \qquad [1]$$

We represent a rigid body transformation F by:

$$F(p) = R(p - C) + C + T = [F1, F2, F3]^T, \qquad [2]$$

where $p = [x, y, z]^T$ is the original point, $p' = [x', y', z']^T$ is the transformed point, R is a rotation matrix, the vector $C = [C_x, C_y, C_z]^T$ is the center of rotation (here gravity center), and $T = [T_x, T_y, T_z]^T$ is the translation. The rotation matrix R is a product of three elementary rotation matrices around X, Y, Z axes:

$$R = XYZ, \qquad [3]$$

where:

$$X = \begin{bmatrix} 1 & 0 & 0 \\ 0 & \cos\theta_x & \sin\theta_x \\ 0 & -\sin\theta_x & \cos\theta_x \end{bmatrix} \quad Y = \begin{bmatrix} \cos\theta_y & 0 & \sin\theta_y \\ 0 & 1 & 0 \\ -\sin\theta_y & 0 & \cos\theta_y \end{bmatrix} \quad Z = \begin{bmatrix} \cos\theta_z & \sin\theta_z & 0 \\ -\sin\theta_z & \cos\theta_z & 0 \\ 0 & 0 & 1 \end{bmatrix}. \qquad [4]$$

If $\Pi = (\pi_1, \pi_2, \pi_3, \pi_4, \pi_5, \pi_6) = (T_x, T_y, T_z, \theta_x, \theta_y, \theta_z)$ is a vector of transformation parameters in 3D space, then we define the alignment error as

$$e(\Pi) = \sum_{i=1}^{N} d^2(F(p_i', \Pi), S_r). \qquad [5]$$

We are looking for a parameter vector Π_0 of the best fit by minimizing the above penalty function over Π.

For minimization process we use Marquardt-Levenberg method for the least square estimation of nonlinear parameters (17). At each iteration the function $d(F(p, \Pi))$ is expanded in a first order Taylor series over Π around the point Π_k. This expansion is used to develop an approximation to $e(\Pi)$ in the vicinity of the same point. The approximation to $e(\Pi)$ has the form:

$$e(\Pi) \approx e_k(\Pi) = e(\Pi_k) + \Delta^T G + \Delta^T A \Delta, \qquad [6]$$

where $\Delta = \Pi - \Pi_k$, G is a vector whose components are given by:

$$G_i = 2\sum_{l=1}^{N} d(F(p_l, \Pi)) \frac{\partial d(F(p_l, \Pi))}{\partial \pi_i}, \qquad [7]$$

where N is the number of test points. Matrix A has coefficients:

$$A_{i,j} = 2\sum_{l=1}^{N} \frac{\partial d(F(p_l, \Pi))}{\partial \pi_i} \frac{\partial d(F(p_l, \Pi))}{\partial \pi_j}. \qquad [8]$$

The computations of vector G and matrix A require the values of $\partial d/\partial \pi$. These are found from the chain rule:

$$\frac{\partial d}{\partial \pi} = \sum_{i=1}^{3} \frac{\partial d}{\partial F_i} \frac{\partial F_i}{\partial \pi} = \left[\frac{\partial d}{\partial F_1} \quad \frac{\partial d}{\partial F_2} \quad \frac{\partial d}{\partial F_3} \right] \left[\frac{\partial F_1}{\partial \pi} \quad \frac{\partial F_2}{\partial \pi} \quad \frac{\partial F_3}{\partial \pi} \right]^T. \qquad [9]$$

For a given point p transformed to a new location p' the distance between it and a point p_0 the closest one belonging to S_r can be given by:

$$d = \sqrt{(x'-x_0)^2 + (y'-y_0)^2 + (z'-z_0)^2} = \sqrt{(F_1 - x_0)^2 + (F_2 - y_0)^2 + (F_3 - z_0)^2}. \qquad [10]$$

If we assume:

$$x' - x_0 = v_x, \; y' - y_0 = v_y, \; z' - z_0 = v_z \qquad [11]$$

then:

$$d = \sqrt{v_x^2 + v_y^2 + v_z^2} \quad \text{and} \quad \frac{\partial d}{\partial F_1} = \frac{\partial d}{\partial v_x} \quad \text{...etc.} \qquad [12]$$

Vector $v = (v_x, v_y, v_z)$, where v_x, v_y, v_z are the values of distances between point p and object S_r along X, Y, Z axes respectively. So, for a given p we compute $\partial d/\partial \pi$ as follows:

$$\frac{\partial d}{\partial \pi} = \left[\frac{\partial d}{\partial v_x}\ \frac{\partial d}{\partial v_y}\ \frac{\partial d}{\partial v_z}\right]\left[\frac{\partial F_1}{\partial \pi}\ \frac{\partial F_2}{\partial \pi}\ \frac{\partial F_3}{\partial \pi}\right] = \left[\frac{v_x}{\|v\|}\ \frac{v_y}{\|v\|}\ \frac{v_z}{\|v\|}\right]\left[\frac{\partial F_1}{\partial \pi}\ \frac{\partial F_2}{\partial \pi}\ \frac{\partial F_3}{\partial \pi}\right]^T, \qquad [13]$$

where $\|v\| = \sqrt{v_x^2 + v_y^2 + v_z^2}$ is the length of the vector v i.e. the distance of p' from S_r.

Thus, according to {13} partial derivatives of $d(F(\Pi))$ over parameters of 3D rigid body transformation are computed in the following way:

$$\frac{\partial d(F(\Pi))}{\partial T_x} = \left[\frac{v_x}{\|v\|}\ \frac{v_y}{\|v\|}\ \frac{v_z}{\|v\|}\right]\begin{bmatrix}1\\0\\0\end{bmatrix} = \frac{v_x}{\|v\|}, \qquad [14]$$

$\frac{\partial d}{\partial T_y}$ and $\frac{\partial d}{\partial T_z}$ are computed analogously.

$$\frac{\partial d(F(\Pi))}{\partial \theta_x} = \left[\frac{v_x}{\|v\|}\ \frac{v_y}{\|v\|}\ \frac{v_z}{\|v\|}\right]\ \frac{\partial R}{\partial \theta_x}\begin{bmatrix}x - C_x\\ y - C_y\\ z - C_z\end{bmatrix} \qquad [15]$$

$\frac{\partial d}{\partial \theta_y}$ and $\frac{\partial d}{\partial \theta_z}$ are computed analogously.

According to {6} the value of Δ that minimizes $e(\Pi)$ (first derivative over Δ has to be equal 0) is found by solving:

$$A\Delta + G = 0. \qquad [16]$$

However, sometimes the approximation of $e(\Pi)$ is not accurate enought, and then the solution of {16} may not converge to the minimum. To avoid this in the Marquardt-Levenberg method Δ is estimated by solvinig:

$$[A + \lambda_k I]\Delta + G = 0, \qquad [17]$$

instead of {16}. I is the identity matrix and λ is a positive scalar. By modyfying the value of λ in each iteration we can assure that $e(\Pi_{k+1}) < e(\Pi_k)$. The initial value of λ, as well as v below are found empirically. Basing on (16) and (12) we used the following implementation of the Marquardt-Levenberg algorithm:

1. Initialize:λ =3, v=10. Initialize parameters Π. Set C, the center of rotation to the gravity center of the test object. Compute d_0=$e(\Pi_0)$. Set τ, the stop criterion.
2. Compute matrices A, G.
3. Find Δ_1 from the equation set: $(A + \lambda I)\,\Delta_1 = -G$, and Δ_2 from: $(A + \lambda/vI)\Delta_2 = -G$.
4. Compute $d_1 = e(\Pi + \Delta_1)$ and $d_2 = e(\Pi + \Delta_2)$.
5. if $\|\Delta_1\| < \tau$ then stop optimization
6. if $d_2 < d_0$

   then

   $\lambda = \lambda/v$, $\Pi = \Pi + \Delta_2$, $d_0 = d_2$, go to step 2.

   else if $d_2 > d_0$ and $d_1 < d_0$

   then

   $\Pi = \Pi + \Delta_1$, $d_0 = d_1$, go to step 2.

   else

   do

   $\lambda = \lambda v$

   Find Δ from the equation set: $(A + \lambda I)\Delta_1 = -G$.

   untill $e(\Pi + \Delta) < d_0$

   $d_0 = e(\Pi + \Delta)$, $\Pi = \Pi + \Delta$, go to step 3.

   endif

   endif

The Marquardt-Levenberg optimization process requires time consuming computations of distances between test points p_i and the reference surface S_r i.e. the vector $v = (v_x, v_y, v_z)$. That is why we precompute a distance map of the reference object, using the algorithm described in (13). The distance map is a 3D array whose entries are 3D vectors from the given voxel to the closest voxel belonging to the reference object. It serves as a look up table, to which we refer during computations. The image representation of the distance map computed for the scalp surface of one of our patients is shown in Fig. 3. The whitest colour indicates the longest distance while the darkest one represents the shortest distance to the surface (black corresponds to the distance=0 i.e. the surface itself). Figure 3b shows a cut away block of this distance map.

The initial guess of transformation Π was found manually using a tool we designed on AVS platform. The test points are transformed manually in (i.e. using mouse), to be located sufficiently close the surface, but without taking a special care of accuracy. The parameters of transformation generated by mouse are accessible in AVS and are transmitted into a procedure performing the alignment, which uses them as the initial transformation. The result of the alignment is displayed on the screen, so we can visually verify if the objects do not fit at all (optimization falls into a local minimum), and if so then repeat the process.

Interpolation

Once electrodes are aligned to the cortex, the interelectrode potentials are computed for the entire surface using spherical spline method. The idea of spherical splines introduced by Wahba (23) was later used for scalp potential mapping by Perrin et al (19), on whose work our computations are based. According to (19) spherical splines allow to interpolate data recorded from a small number of irregularly disposed electrodes, better than the other interpolation techniques, and give continuous surface, as well as better estimate of the locations of extrema not connected with electrode locations. There are methods computing potential distribution more relevant than spherical splines in some cases. The choice of algorithm always depends on what electrophysiogical phenomena one wants to study. Any other algorithm can be introduced into our system just by replacing this module with the other one.

Let z_i be the potential value measured at i-th electrode e_i whose spherical projection is E_i (i=1,2...n). $U(x,y,z)$ is the calculated value that interpolates potential z in point $P(x,y,z)$ belonging to the cortical surface, and having the spherical projection E. $U(x,y,z)$ is computed as follows:

$$U(x,y,z) = c_0 + \sum_{i=1}^{n} c_i \times g(\cos(E,E_i)); \qquad [18]$$

c_i are solutions of the equation system:

$$\begin{aligned} G \times C + T \times c_0 &= Z, \\ T^T \times C &= 0, \end{aligned} \qquad [19]$$

where:

$T = [1,1...,1]^T$, $C = [c_1, c_2,...,c_n]^T$, $Z = [z_1, z_2,...,z_n]^T$, $G = [g_{ij}] = [g(\cos(E_i E_j))]$,

$\cos(E_i E_j)$ denotes cosine of angle between the spherical projections $E_i E_j$ of electrodes e_i, e_j.

$\cos(E_i E_j)$ denotes cosine of angle between the spherical projections $E_i E$ of electrode e_i, and point P.

The function g(x) is defined as:

$$g(x) = \frac{1}{4\pi} \sum_{n=1}^{\infty} \frac{2n+1}{n^m (n+1)} P_n(x), \qquad [20]$$

where P_n is n-th degree Legendre polynomial. Basing on (19) we used n=7, m=4. For each voxel belonging to the surface the U value is computed.

Subsequently, values of U are normalized into integer values of the range (0,255), in order to assign colours to them.

Fusion

The next step after registration required for simultaneous rendering of data sets gathered with various techniques (modalities) is their fusion. In the presented work this step is performed on SGI/Sun platform with the use of AVS (Advanced Visual System) enhanced with our software modules. AVS includes a tool called *geometry viewer*, which provides combination of many objects into a single scene, their surface/volume rendering and manipulation. As a result of interpolation we obtained values representing the potential for each voxel belonging to the cortex surface. The cortex surface resides inside a cuboid (volume bounds) covering the input volumetric data set (sequence of MR crossectional images). The inside of this cuboid is filled in the following way: all voxels belonging to a line determined by a voxel of the surface and centroid of the brain are assigned a colour value computed for this voxel. This procedure is performed for all surface voxels. The computed volume is combined in *geometry viewer* with the other volume (of the same size) containing segmented cortex surface. The surface comes from the output of the *isosurface* module. The *isosurface* module gets on its input a volumetric data set (here a sequence of MR images), tracks the surface of an indicated level and passes it to the output. This way a scene of colour distribution of electrical potential on the surface is generated (see Figures 4, 5).

3. Clinical results

Two subjects were studied. Subject 1 suffered from epileptic seizures, so her EEG maps were analyzed to observe the extent of abnormal discharges. Subject 2 had a tumor located in the right frontal lobe. We studied his sensory evoked potentials to observe extents and locations of areas of electrical potential generations and their spatial relations to the tumor extent.

Two sets of 20 electrodes were aligned with scalps of our 2 patients. The average distance errors (defined as average distance between test points and the reference object) were: 2.57 [pix], 3.07 [pix]. Since the scale was 1mm/pix they were: 2.57 [mm], 3.07 [mm]. Potentials were interpolated over the entire cortex surface and rendered as described in sections: *Interpolation* and *Fusion*.

Figure 4 shows the distribution of potential values on the entire cortex surface for Subject 1. Since the patient was on pharmacological treatment we dealt with electrical activity suppression induced by drugs. Figure 4 presents distribution of electrical activity on the patient's cortex in 3 samples selected from 9 min EEG recordings to demonstrate the character of discharges. MRI itself did not indicate any pathological changes. Abnormal discharges appeared both in right and left frontal lobes. The right lobe abnormal discharges were more frequent but their amplitudes were smaller (about 20 μV) than those of the left frontal lobe (about 30 μV). The right lobe discharges demonstrated also a smaller extent. In Figure 4a we can observe a map representing electrical activity distribution in one of the samples when such discharges occurred in the right frontal lobe (red colour) and a little bit of the temporal lobe. Sometimes they are transmitted to the left frontal and temporal

lobes, where they cover a bigger extent. Figure 4b shows the transition of the discharge from the right to the left hemisphere. Figure 4c presents the example of discharge in the left frontal/temporal lobe. These results may suggest the source of abnormal discharge is in the right frontal lobe, though the left frontal and temporal lobes are also impaired.

Figure 5 shows the distribution of potential values on the entire cortex surface of Subject 2, on whom SEP studies were performed. His right and left median nerves were stimulated with 5-7mA current pulses. The right median nerve stimulation gives N20 potential of latency 34ms and extent presented in Fig. 5a (blue colour). The left median nerve stimulation evokes N20 potential also of 34ms latency close to the area of left hand projection (fig. 5b), but in comparison to the potential in Fig 5a it covers a much smaller extent, what suggests generation of this potential in the right hemisphere is impaired. Left median nerve stimulation evokes also untypical late potential P80. It is generated in the right frontal lobe in the tumor area (Fig. 5c). Its spatial relation to the tumor extent is presented in Figure 5d. Potential P40 does not appear explicit during the left median nerve stimulation, although it marks on a rising edge of an untypical late P80 potential.

All maps were in a good agreement with maps created with a conventional BEAM technique used in our Lab for diagnosis (Walerian et al. (24),(25)).

4. Discussion

The presented results demonstrated the usefulness of the method for analysis of the extent of electrical signal propagation and generation and its changes in the relation to individual anatomical structures. This technique allows to observe the electrical activity distribution on the individual cortex surface in 3D space. It allows to use arbitrary positions of electrodes, if one is able to scan their 3D coordinates. In the case of Subject 1 it provided assessment of the influence of pharmacological treatment on the change and character of EEG signals, as well as comparison of created maps with other ones obtained at different time. In the case of SEP studies performed on the second patient the method allows to assess the extents of areas of potential generation and their spatial relation to the tumor extent.

The distance based alignment technique used here for data registration doesn't require any external fiducial markers (headholders, frames, electrodes themselves) to be fixed on a patient's head. It makes the method easy to apply, especially when electrophysiological and MRI examinations are performed at different places and times. Thus, it gives also opportunity to compare EEG/EP performed at different times.

The technique used for the alignment suits the case when we deal with partially missing data or experimentally obtained data sets (here a subset of scalp surface points). Since it is based on a measure of a disparity between two geometrical objects, it minimizes the distances, no matter how different they are. The error of the method basically depends on 3 components: i) alignment error, ii) interpolation error, iii) error of measurement of electrode positions. i) The alignment error is a function of a number of test points used for the alignment, stopping

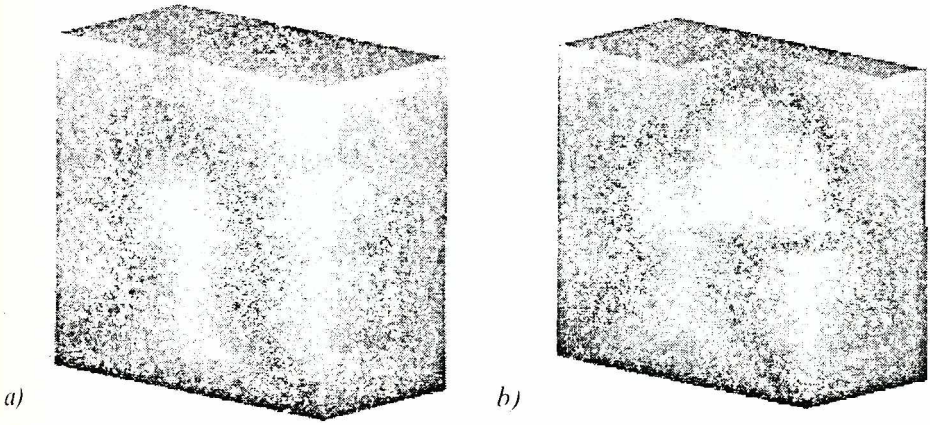

Figure 3. *Image representation of 3D distance map computed for the scalp surface of one of our patients. The darkest colour represents the surface itself (distance=0). The whitest colour indicates the farthest distance. a) Cuboid including the surface for which distance map was computed. b) Cut away block of 3D distance map. Distance map inside the object is visible*

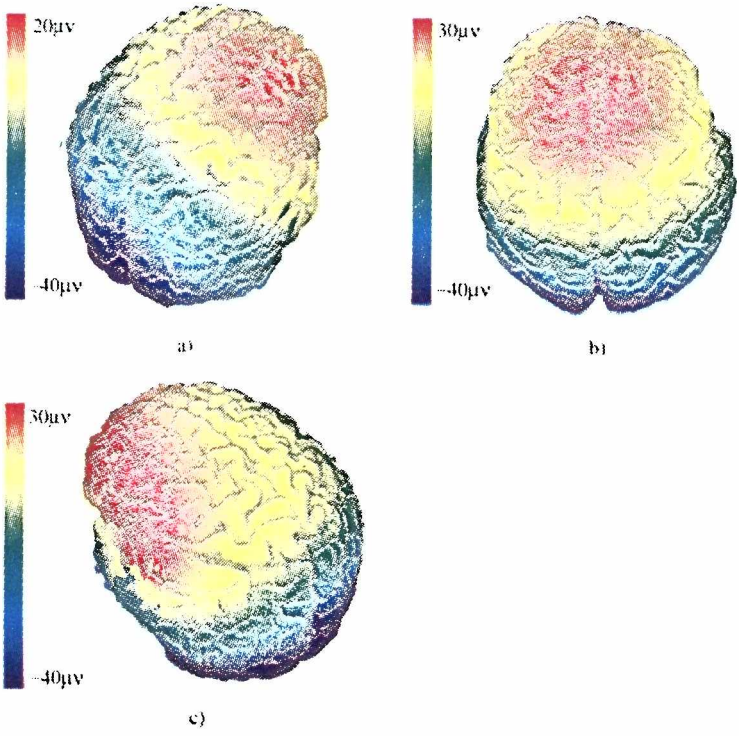

Figure 4. *Selected samples from EEG recordings of Subject 1. a) Discharge in the right frontal lobe (red colour) of amplitude about 20mV. b) Transition of discharge the right to the left frontal lobe. c) Discharge propagated to the left frontal lobe (red colour) of amplitude about 30mV.*

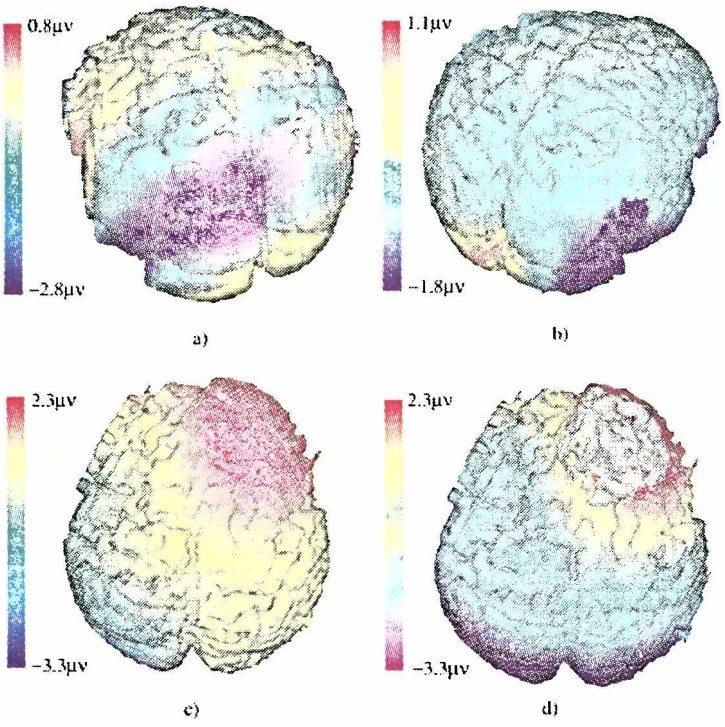

Figure 5. *Sensory Evoked Potential examination of Subject 2. a) Right median nerve stimulation. Distribution of N20 potential, latency 34ms. b) Left median nerve stimulation. Distribution of N20 potential, latency 34ms. Maximum amplitude component covers smaller and a little different extent in comparison to a). c) Left median nerve stimulation, P80potential, latency 80ms . d)Left median nerve stimulation. Distribution of P80 potential and tumor extent (grey scale).*

criterion and the initial guess as reported in (13). To reduce the error one should increase the number of test points (i.e. to scan more points belonging to the scalp surface) and decrease the stopping condition. Both will imply the increase of optimization time. In the case of our data and for stopping criterion 0.1 pixel for translation and 0.003 radian for rotation, we obtained the average distance error in the range of 2-3 pixels (for the scale in our images: 1mm/pixel it means 2-3mm). Of course, the map error can be bigger since the optimization process may fall into local minima. This can be reduced by scanning more points, which are characteristic, e.g. from ears or nose. In our system it is verified by visual inspection. The Monte Carlo tests for accuracy of the method performed on synthetic objects are reported in (13). ii) An interpolation error component decreases together with the increase of the number of control points. We used a standard 10-20 electrode system because it is commonly used in clinic and it was available in our Lab. According to (19) for our data: 20 control points (electrodes) and eccentricity 0.29, the RMS error of the

spherical spline interpolation is 0.8%. iii) The error of measurement of electrode positions, as well as other control points depends on accuracy of a 3D scanning device.

In the proposed solution scalp recorded potentials are just overlapped on the cortical surface. This potential distribution has lower resolution than one which appears on the cortex surface due to distortion of electrical signal during propagation from cortex to scalp surface. Thus, to get a distribution closer to the reality one should employ a deblurring technique. Some deblurring methods have been proposed by Dale (6), Babiloni (1), Yvert (26). The resolution of potential distribution can be also improved in the acquisition phase by increasing the number of scalp electrodes. But on the other hand according to (10) and (2) the number of electrodes has its upper limit: to avoid spatial aliasing the interelectrode distance must not be smaller than 2,5 cm.

5. Conclusion

A method providing registration and fusion of electrophysiological and anatomical data has been developed. The alignment technique can register any surface of known 3D coordinates of points (voxels) with a subset of points scanned from this surface. The method successfully assists in localization of areas of pathological activity in the brain with respect to individual topography of the cortex. The use of distance based alignment technique creates an opportunity for not fixing any fiducial markers on a patient's head, which makes it promising for numerous clinical examinations.

Acknowledgements

MRI examinations of our subjects were performed with Siemens Magnetom 1.5T scanner in Nuclear Medicine and Magnetic Resonance Division of Wojewodzki Szpital Brodnowski (Warszawa, ul. Kondratowicza 8).

References

[1] Babiloni F., Babiloni E. C., Carducci F., et al.,"High resolution EEG: a new model-dependent patial deblurring method using a realistically-shaped MR-constructed subject's head model", Electroenceph. clin. Neurophysiol., 102, pp. 69-80, 1997

[2] Babiloni F., Cracas S., Johnson P. B., et al.,"Computerized mapping system of cerebral evoked potentials", Comp. Biomed. Res., vol 23, pp. 165-178, 1990

[3] Besl P., McKay N. D.,"A method for registration of 3-D shapes", IEEE Trans. on Pattern Analysis and Machine Intel., vol. 14, no. 2,1992)

[4] Borgefors G.,"Distance transformations in arbitrary dimensions", Comput. Vision, Graphics, Image Processing, vol. 27, pp. 321-345, 1984

[5] Borgefors G.,"Hierarchical chamfer matching: a parametric edge matching algorithm", IEEE Trans. on Pattern Analysis and Machine Intelligence, vol. 10, no. 6, pp. 849-865, 1988

[6] Dale A., Sereno I.,"Improved localization of cortical activity by combining EEG and MEG with MRI cortical surface reconstruction: a linear approach"- J. Cogn. Neurosc., 5:2, pp. 162-176, 1993

[7] Danielsson P. E.,"Euclidean distance mapping", Comp. Graphics and Image Processing, vol. 14, pp. 227-248, 1980

[8] Duffy F. H. (ed),"Topographic mapping of brain electrical activity", Butterworths, Boston 1986

[9] Gencer N. G., Williamson S. J., Gueziec A., Hummel R. ,"Optimal reference electrode selection for electric source imaging", Electroenceph. clin. Neurophysiol., 99, pp. 163-73, 1996

[10] Gevins A. S.,"Analysis of the electromagnetic signals of the human brain: milestones, obstacles and goals", IEEE Trans. Biomed. Eng. BME31, 833 (1984)

[11] Grzeszczuk R., Kim K. Tan, Levin D. N., Pelizzari C. A. et al.,"Retrospective fusion of radiographic and MR data for localization of subdural electrodes", J. Comp. Assist. Tomog., vol. 16(5), pp. 764-773, 1992

[12] Jiang H., Robb R. A., Holton K. S.,"A new approach to 3-D registration of multimodality medical images by surface matching", SPIE vol. 1808 (Visualization in Biomedical Computing), pp. 334-341, 1992

[13] Kozinska D., Tretiak O., Nissanov J., Ozturk C.,"Multidimensional alignment using Euclidean distance transform"- CVGIP Graphical Models and Image Processing,vol. 59, No 6, 1997, In Press

[14] Lamer R., Lacroix D., Meunier et al.,"Imaging of the electrical activity of the brain: a colour display of EEG local coherence", 16 th IEEE EMBS Conference, vol 2, 1994

[15] Lavanlle S., Szeliski R.,"Recovering the position and orientation of free form objects from image contours using 3D distance map", IEEE Trans. PAMI, vol. 17(4), pp. 378- 390, 1995

[16] Levin D. N., Pelizzari C. A., Chen G. T. Y., Chen C. T., Cooper M. D.,"Retrospective geometric correlation of MR, CT, and PET images", Radiology, vol. 169, pp. 817-823, 1988

[17] Marquardt D. W., "An algorithm for least squares estimation of nonlinear parameters" J. Soc. Appl. Math., vol 11, No 2, June 1963

[18] Pellizari C. A., Chen G. T. Y., Spelbring D. R., Weichselbaum R. R., Chen C. T. ,"Accurate three-dimensional registration of CT, PET, and/or MR images of the brain", J. Comp. Assist. Tomog., vol. 13(1), pp. 20-26, 1989

[19] Perrin F., Pernier J., Bertrand O., Echallier F., "Spherical splines for scalp potential and current density mapping", Electroenc. and Clinical Neuroph., vol 72, pp. 184-187, 1989

[20] Rosenfeld A. and Pfaltz J.,"Distance functions on digital pictures", Pattern Recognition, vol. 1, pp. 33-61, 1968

[21] Sung-Schik Yoo, Guttman C., Ives J., Panych L., Kikinis R., Schomer D., Jolesz F.,"3D localization of surface 10-20 EEG electrodes on high resolution anatomical images" Electroenceph. clin. Neurophysiol., 102, p. 335-339, (1997)

[22] Elsen van den P. A., Pol E. J. D., Viergever M. A.,"Medical image matching - a review with classification", IEEE Engineering in Medicine and Biology, vol. 3, pp. 26-39, 1993

[23] Wahba G.,"Spline interpolation and smoothing on the sphere", SIAM J. Sci. Stat. Com put., vol. 2, No 1, 1981

[24] Walerian P., Purska E., Tarnecki R., Mempel E. ,"New Mapping program for PC computer", Knowledge, Information and Medical Education, Elselvier Science Publishers B.V., IMIA, 1991

[25] Walerian P., Tarnecki R. ,"Computer mapping techniques for analysis of scalp potential distribution", Biocyb. and Biomed. Eng., vol 11, No 1-2, pp. 91-96, 1991

[26] Yvert B., Bertrand O., Echallier J. F., Pernier J. ,"Improved dipole localization using local mesh refinement of realistic head geometries: an EEG simulation study", Electroenceph. clin. Neurophysiol., 99, pp. 79-89, 1996E